Exceptional Heat and Basin-Scale Connections in the Kuroshio-Oyashio Region in the Early 2020s

Shoshiro Minobe, Faculty of Science, Hokkaido University, Sapporo, Japan

(minobe@sci.hokudai.ac.jp)

Abstract

This study investigates recent extreme conditions in the North Pacific, which began in the late 2010s and have intensified significantly by 2024, focusing on the Kuroshio-Oyashio region. The anomalies appear to have originated in the western North Pacific, linked to changes in the Kuroshio and Oyashio currents, while those in the eastern North Pacific began to develop in a separate and distinct region. Sea surface temperature anomalies in the Kuroshio-Oyashio region have reached record-breaking levels, with deviations up to 6°C above the 1990–2019 average. Subsurface temperatures have also increased notably, accounting for 15.8 % and 11.8 % in the western and eastern North Pacific (27.6% combined) of the global ocean heat content increase in the 0–300 m layer between 2020-2024 and 2010s. Extreme marine heat waves occurred in coastal water near Japan in 2023-2024, resulting in the largest area-day fraction of extreme MHWs among world basins. In the 2020s, Kuroshio water anomalously intruded northward to approximately 42°N along Japan's coast, forming a loop-like pattern with a southward return flow, while the Kuroshio Extension, over a wider zonal extent, also shifted northward by about 1.3° in latitude. These oceanic anomalies are likely influenced by wind changes, with Sverdrup theory suggesting weakened subtropical gyres and a northward shift of the subtropical-subpolar gyre boundary. Further research is needed to fully understand, monitor, and predict these changes and their impacts on regional ecosystems.

Introduction

The Earth's climate has exhibited exceptional warmth from mid-2023 through the present (February 2025). This abnormal warmth is exceptional, even when considering the ongoing progression of global warming. In July 2023, the UN Secretary-General declared that the climate was no longer in a state of global warming, but instead in "global boiling." In 2024, annual mean air-temperature has exceeded 1.5°C threshold above pre-industrial level for the first time[1]. The exceptional warming in 2023-24 is likely to be related to the acceleration of the global warming with exceptionally strong Earth's Energy Imbalance in early 2023 combined with heat release from the subsurface ocean to

---

[1] https://climate.copernicus.eu/copernicus-2024-first-year-exceed-15degc-above-pre-industrial-level (access February 12th, 2025)

near surface and to the atmosphere due to the 2023/24 El Nino (Goessling et al., 2025; Minobe et al., 2025).

Among the world's oceans, the Kuroshio-Oyashio (K-O) region has experienced a particularly pronounced warming during this exceptional heat period of 2023-2024. **Figure 1** shows the sea-surface temperature (SST) anomalies for one year, from July 2023 to June 2024, relative to the 1990-2019 climatology, based on OI-SST version 2.1 (Huang et al., 2021). In the K-O region, anomalies exceeding 6°C are observed, consistent with a recent study by Sugimoto et al. (2025). No other ocean region shows such high temperature anomalies. Anomalies remain below 2°C across most other regions of the global ocean, and anomalies reaching 3°C occurred only in a narrow area of the Gulf Stream outside of the North Pacific (NP). Therefore, it can be said that the K-O region is the focal point of global boiling in 2023-24. Given the K-O region's significant role in ocean-atmosphere interactions (Larson et al., 2024; Oka et al., 2023; Sasaki & Ito, 2024; Sato et al., 2024; Sugimoto et al., 2021) and heat transport (Kawakami et al., 2022), its investigation is of critical importance from a global perspective.

Prior to this exceptional warming in 2023-2024, several notable anomalous conditions were reported in the K-O region, including marine heat waves (MHWs). Marine heatwaves have garnered increasing attention in recent years (e.g., Capotondi et al. (2024)), and it has been pointed out that their frequency, intensity, and duration are increasing due to global warming (Frölicher et al., 2018). In the 2010s, frequent MHWs have occurred in the Kuroshio-Oyashio during the summer (Miyama et al., 2021), with the start of the MHWs being associated with the increase of fish-catch of yellow-tail in Hokkaido. The Kuroshio has been in a large meander since August 2017, which has persisted until now[2]. This is the longest period of a large meander since observations began in 1961, could be related to the oceanic circulation changes driven by anomalous atmospheric circulation (Qiu et al., 2023). The strength of the Oyashio has been decreasing according to trend analysis from 1982 to 2016 (Kawakami et al., 2024). The formation rate of the North Pacific subtropical mode water substantially decreased in the period 2018-2021 (Sheng et al., 2024). The North Pacific heat content increased in the 2010s (Kawai et al., 2023). MHWs occurred in 2020 in the western NP (Kuroda & Setou, 2021) and in 2022-2023 in the Oyashio region, accompanied by a near surface dissolved oxygen decrease of associated abnormal Kuroshio water intrusion (Kawai et al., 2024).

Since Kuroshio and Oyashio are the western boundary currents, their variability may be related to the changes in the NP basin. In particular, Rossby waves generated in the eastern-central NP can influence the western boundary currents (Ceballos et al., 2009; Kawakami et al., 2023; Qiu, 2003; Sasaki et al., 2013; Sasaki & Schneider, 2011; Taguchi et al., 2007). Although most previous studies focused on baroclinic Rossby waves, barotropic propagation signatures associated with the Pacific Decadal Oscillation (PDO) were also reported (Andres et al., 2011).

The unprecedented warming observed in 2023-24 underscores a critical need for substantial research. To start, it is essential to document recent changes in the K-O region and their relationship to variations in the NP basin. This paper aims to provide timely documentation of these exceptional conditions through analyses of observational data. A key focus of this study is to determine whether the anomalous heat in the K-O region and the broader North Pacific has significant implications for ocean heat uptake in the context of global warming. Understanding of MHWs in these years is important for society. Also, understanding how current changes relate to temperature shifts is especially crucial in the western NP, where narrow SST anomalies shown in **Fig. 1** suggest that currents play an important role. Given that the Kuroshio and Oyashio are wind-driven currents, this

[2] https://www.data.jma.go.jp/kaiyou/data/shindan/b_2/kuroshio_stream/kuroshio_stream.html (Access October 31st, 2024)

study examines the relationship between these oceanic anomalies and changes in wind forcing over the North Pacific.

The rest of the paper is organized as follows. In section 2, data and methods used in this paper are explained. In section 3, changes in temperature including ocean heat content, conditions of MHWs, ocean circulation anomalies in the western NP, and the relations to atmospheric wind forcings are investigated. Summary, discussion and conclusions are given in Section 4.

2. Data and Methods

In this study, the following datasets are analyzed: Optimal-Interpolation (OI) SST version 2.1 (Huang et al., 2021); The Ocean Reanalysis Version 5 (ORAS5) of European Centre for Medium-Range Weather Forecasts (ECMWF) (Zuo et al., 2019); ocean analyses of EN4.2 (Good et al., 2013), Japan Meteorological Agency (JMA) version 3.7.1 (Ishii et al., 2017), and Institute of Atmospheric Physics (IAP) in China version 4 (Cheng, et al., 2024). Satellite-derived sea-surface height (SSH) analyzed and distributed by Copernicus Climate Change Service is also examined. To understand the atmospheric forcings, sea-level pressure and wind-stress of the fifth generation reanalysis dataset produced by the European Centre for Medium-Range Weather Forecasts (ECMWF) (ERA5) (Hersbach et al., 2020) is analyzed.

For the OI SST, daily data are downloaded and monthly mean from the daily data are calculated. For other data, monthly data are downloaded and analyzed. The horizontal resolution is 0.25° for OI-SST, SSH, and ERA5 data, and also ORAS5 data are around 0.25° on a curve-linear grid. Other data are gridded on a 1° grid. Climatology is calculated for a 30-year period from 1990 to 2019. Also, epoch differences between the 2020s and 2010s are calculated in some analyses.

The ocean heat content (OHC) is calculated from three-dimensional potential temperatures (ORAS5 EN4.2) or from in-situ temperatures of the JMA data and respective salinity data using Thermodynamic Equation Of Seawater - 2010, Gibbs Seawater python package known as TEOS-10 GSW toolkit[3]. We also use OHC data for 0-300 m layer thickness of the IAP data. The heat content calculation of ORAS5 is conducted on the original native grid. Most of the data are analyzed through December 2024. However, SST and ORAS5 OHC data are analyzed through March 2025, while SSH data are only available through November 2024, based on two-satellite delayed-time data up to June 2024 and all-satellite near-real-time data thereafter.

MHWs are analyzed following the methodology of Hobday et al., (2016; 2018) using OI-SST. Daily SST climatologies are calculated based on data from 1990 to 2019, applying an 11-day running mean for smoothing. The 90th percentile of SST anomalies is determined using an 11-day moving window at each grid point. Regions with sea ice concentration exceeding 15% are excluded by assigning missing values to the corresponding SSTs. MHW intensity is classified based on observed SST anomalies, with moderate, strong, severe, and extreme MHWs corresponding to anomalies exceeding one, two, three, and four times the 90th percentile threshold, respectively, for at least five consecutive days.

Air-sea heat fluxes are not analyzed in this paper, because a large discrepancy is found in heat fluxes among three datasets including ERA5, Japanese Reanalysis for Three Quarters of a Century

[3] https://teos-10.github.io/GSW-Python/ (access October 31st, 2024)

(JRA3Q) (Kosaka et al., 2024) and (Modern-Era Retrospective Analysis for Research and Applications, Version 2 (MERRA2) (Gelaro et al., 2017). The large discrepancy in heat fluxes among different data products for NP variability is consistent with Kawai et al., (2023). Recent studies by Sato et al., (2024) and Hu et al., (2024) suggested that the air-sea heat fluxes act to damp the SST anomalies in recent changes near Japan and over NP, respectively.

To understand the influence of wind forcing on ocean circulation anomalies, the Sverdrup theory is used. The meridional Sverdrup transport is given by

$$\beta V = (1/\rho)\, \nabla \times \boldsymbol{\tau} \quad (1)$$

where β represents the latitudinal variation of the Coriolis parameter, V is the northward transport (including both geostrophic and Ekman transports), $\boldsymbol{\tau}$ is the surface wind stress vector, and ρ is the density of seawater. When the Sverdrup transport approximation holds, characteristics of information propagation is zonal, and timescale of variability is longer than the time for propagation, the zonal integration of Sverdrup transport yields the meridional return flow at the western boundary (WB). As emphasized by Wunch (2011), the Sverdrup transport is only valid where vertical velocities in the deep ocean can be ignored. While this condition may hold in the subtropics, it does not in the subarctic regions due to weak stratification (Wunch, 2011). Also, deviation of propagation of the Rossby wave characteristics from zonal direction is generally large in higher latitudes in baroclinic modes (e.g. Nakamura 1998). Therefore, it is important to remain cautious of the limitations of Sverdrup theory especially in the subarctic NP.

Given the limitations of the Sverdrup theory as a coarse approximation, we use it here to examine overall tendency by combining the use of Empirical Orthogonal Function (EOF). The Sverdrup transport, as defined in Eq. (1), is calculated at each grid point using ERA5 data and integrated zonally across the North Pacific basin. The WB transport is assumed to have the same magnitude as the meridional Sverdrup transport, but in the opposite direction. This estimated WB transport is analyzed using EOF analysis, yielding a spatial pattern as a function of latitude and a corresponding temporal component. As will be shown later, several features identified in the EOF analysis of Sverdrup transport align with observed transport changes.

3. Results

3.1 Temperature Change

Let us first examine the temporal evolution in the North Pacific leading up to the SST in **Fig. 1**. **Figure 2** shows SST anomalies from 2010 to 2024. The last three-years (2022-2024), strong positive temperature anomalies occurred between 30°N and 50°N across the basin. These SST anomalies appear to develop from the western and eastern NP separately. SST patterns in 2020 and 2021 in the eastern NP are somewhat similar to SST anomalies of the Blob in 2015 and 2016 (Amaya et al., 2020), but recent anomalies (e.g., 2021) do not reach the North American coast as observed in 2016. Compared with SST anomalies in the eastern NP, the SST anomalies in the western NP are much more narrowly concentrated to the K-O region and the Japan Sea, clearly suggesting that ocean currents in the western NP played a role in shaping SST anomalies.

How were SST variations related to the subsurface temperature anomalies? Yearly sampled 0-300 m OHC anomalies are shown in **Fig. 3.** This figure indicates that the OHC anomaly development is consistent with the SST anomaly qualitatively, as positive and negative anomalies of OHC corresponding positive and negative anomalies of SST, respectively. Also, anomalies in the 2020s began to develop in western and eastern North Pacific separately in 2020. Although previous studies suggested that the jet-trapped, westward propagating Rossby waves play an important role in variability of the Kuroshio Extension (Sasaki et al., 2013; Sasaki and Schneider, 2011), westward propagating signal is not prominent in the development of the OHC anomalies in the western NP. Rather, the SST and OHC anomalies in the western NP appear to expand eastward in the late 2010s and the early 2020s, suggesting an important role of advection. It is interesting to note that although the OHC anomaly in the eastern NP in 2021 is somewhat similar to that in 2016 consistent with SSTs in **Fig. 2**, the further developments in the following years are quite different. In the 2010s, the eastern NP OHC anomalies substantially weakened in two years by 2018, but in the 2020s, strong OHC anomalies remained and merged with the OHC anomalies extending from the western NP.

The contrasting feature in the western and eastern NP is also evident in a time series comparison between area-integrated 0-300 m OHC and area-averaged SST (**Fig. 4**). The time series are scaled in a manner that SST and OHC anomalies in the beginning and end of the periods are comparable in the figure. In the western NP, the warmings in the late 2010s and in the 2020s are similar between SST and OHC. On the other hand, SST in the eastern NP exhibited spike-like warmings around 2015 associated with the original Blob or the Blob 1.0 and also in 2019-2020 with the Blob 2.0 (Amaya et al., 2020) in both cases without similar spikes in the OHC, which exhibits a trend-like warming from the early 2010s to present. Consequently, trend-like subsurface warming occurred in the late 2010s and 2020s both in the western and eastern NP, and additional surface warming spikes occurred in the eastern NP.

Next, we examine the global pattern of recent OHC warming to determine whether OHC warming in the NP stands out, similar to SSTs. **Figure 5** shows the 0-300 m OHC difference between the periods 2020–2024 and 2010–2019. The NP exhibits the most intense warming, especially in the K-O region and the Japan Sea. The warm OHC anomalies in the central-eastern NP are related to anomalies originating from the eastern NP, as shown in Fig. 3. The pattern exhibits strong amplitudes around the subarctic front in the western NP and subtropical front in the eastern NP, reminiscent of SST changes that occurred in the 1940s and 1970s climatic regime shifts over the NP (Nakamura et al., 1997; Minobe & Maeda, 2005) associated with phase reversals of the PDO (Mantua et al., 1997) (see also a review by Newman et al., (2016)). Indeed, the spatial patterns of SST and OHC changes are generally consistent with the PDO pattern. The PDO index, which has been available since 1854, has been negative in the 2020s and reached its lowest value in October 2024[4]. Outside the NP, relatively strong warm anomalies are observed in the western tropical Pacific, associated with the three-year La Niña events from 2020 to 2023.

The vertical penetration of the temperature anomalies in the western and eastern NP exhibits a distinctive difference (**Fig. 6**). In the western NP, anomalies penetrated to deeper depths with narrower meridional distribution than in eastern NP. In the longitudinal bands 150°-160°E and 160°-170°E, meridionally narrow anomalies occur around 35°N, roughly the latitude of the Kuroshio Extension, with the maximum around 400-500 m depth. At the same time shallower anomalies occur 40°-45°N, corresponding to the subarctic frontal zone (Kida et al., 2015). The potential temperature anomalies in the eastern NP are shallower, as warmings stronger than 1°C are limited to the upper 200 m depth, occupying a wide meridional extent from 30°-50°N. This pattern in the eastern NP suggests that the warming was primarily driven by local atmospheric forcing rather than by variations

[4] https://www.ncei.noaa.gov/access/monitoring/pdo/ (access 2025/04/14)

in ocean currents. Further research is needed to elucidate how temperature variations are related to changes in the ocean's structure, such as mixed layer and water masses (e.g., Amaya et al., 2020; Nishihira and Sugimoto, 2024).

It is informative to quantify the OHC change in each basin. Table 1 shows global and regional OHC change between 2020s (2020-2024) and 2010s (2010-201) in 0-300 m. The world ocean is first divided into three latitudinal bands: 20°N–90°N (referred to as the Northern Hemisphere, NH, for simplicity), 20°S–20°N (tropics), and 20°S–90°S (Southern Hemisphere, SH). Note that the areas of these three bands are uneven due to the larger land masses in the NH, as shown in the area share column. Within the NH, we further divide into sub-regions, specifically the western NP, eastern NP, and North Atlantic. Half of the global OHC change occurred in the NH, despite its area representing only a quarter of the global ocean.

The 0-300 m OHC change shares in the western NP and eastern NP are 15.8 % and 11.8 %, respectively, for the global OHC change (Table 1). Therefore, the NP contributed more than a quarter (27.6%) of the global ocean OHC change, despite the small area share (11.5%). The OHC change per unit area is especially strong in the western NP associated with the strong OHC changes in the K-O region. Consequently, the NP makes a substantial contribution to the global OHC change, with a notable distinction between the western and eastern NP. In the western NP, OHC changes are concentrated in a narrow region due to the influence of the K-O, while in the eastern NP, changes are spread across a wider area.

The importance of the NP does not strongly depend on the selected depth range. When the depth range is extended from 0–300 m to 0–700 m, the global share of OHC change in the western and eastern NP decreases to 10.9% and 9.9%, respectively, yet together they still account for 20%. In contrast, if the depth range is reduced to 0–100 m, the shares in the western and eastern NP increase to 20.1% and 11.4%, respectively, exceeding 30% combined. This indicates that while the NP's contribution is more pronounced in shallower layers, it remains substantial even at greater depths.

3.2 Marine heat waves

It is important to further examine the severe ocean warming of the 2020s in the context of MHWs. The identification of MHWs accounts for the climatological distribution of SSTs (Hobday et al., 2016; 2018). The KO region is known for its strong SST variability compared to the open ocean. Consequently, extreme warming in this region does not necessarily translate to extreme conditions when assessed within the MHW framework.

To evaluate the overall interannual developments of MHWs, area-day fraction for each ocean basin is introduced as

$$F_C(y_r) = \frac{1}{SJ}\int_s \int_j^J M_C(s, j, y_r)\, dj\, ds , \quad (2)$$

where F is the fraction as a function of year (y_r) for MHW of a specific category, C is the MHW category, s is the spatial grid point, S is the whole area of the basin, j is the Julian day, J is the number of days of the year (365 or 366), and M_C is unity if the MHW of corresponding category occurs or zero otherwise. Therefore, this metric is an area and time integration of grid points where MHWs of a certain category for each basin and each calendar year, divided by the area of the basin and days of the year, resulting in an annually sampled index having value between 0 and unity (100%).

The widely used MHW categories extend up to the extreme level. However, as will be shown shortly, MHWs exceeding this intensity—specifically, those surpassing five times the 90th percentile SST anomaly value described in Section 2—also occurred. In this study, we refer to such events as *ultra* MHWs.

Figure 7 shows the area-day fraction for each basin and for each category of MHW. The moderate and strong MHWs exhibit an overall increasing trend. During the 2010s, a prominent peak is particularly notable in the eastern NP, where MHW fractions were much larger than in other basins associated with the Blobs. In the 2020s, MHWs have increased across all basins compared to the 2010s. The increase occurred earlier in the western and eastern North Pacific than in other basins, whereas in 2023 and 2024, the North Atlantic exhibited the highest MHW fractions among all basins in the moderate and strong categories.

As MHW intensity increases from severe to extreme and ultra, the western NP shows significantly higher MHW fractions than other basins in 2023 and 2024, with one exception: in 2023, the North Atlantic had a slightly larger fraction of severe MHWs than the western NP. Furthermore, in 2024, the extreme MHW fraction in the western NP was several times higher than the second-highest fraction, observed in the North Atlantic. For ultra MHWs, the fraction in the western NP was an order of magnitude greater than that of any other basin in 2024.

The global distribution of MHWs in 2023 and 2024 is shown in **Fig. 8**, illustrating the percentage of days experiencing marine heat waves of each category or higher. Consistent with the area-day fraction in **Fig. 7,** moderate MHWs were most widespread in the North Atlantic. A recent study reported that the anomalous warming in the subtropical eastern North Atlantic in 2023 was driven by abnormally enhanced shortwave radiation due to reduced cloud cover, combined with exceptionally shallow mixed layers (Minobe et al., 2025). In the NP, MHWs occurred in relatively narrow regions, suggesting that ocean circulation anomalies play a crucial role in MHW development in this basin

To examine the MHW patterns in the North Pacific in greater detail, **Fig. 9** shows the percentage of days experiencing MHWs within the basin. Moderate MHWs occurred around Japan, the subarctic front region, and the subtropical eastern North Pacific. Strong MHWs were primarily confined to the east of Japan and the subarctic front region. Severe MHWs exhibited two local maxima: one east of Tohoku, the northern part of Japan's main island, and another east of Hokkaido Island. In the latter region, extreme MHWs were also prominent, with ultra MHWs occurring as well. The occurrence of severe and extreme MHWs near the coast suggests significant impacts on coastal marine ecosystems and fisheries.

3.3 Ocean Circulation Changes in the western North Pacific

The results in the previous sections indicate that the NP experienced unprecedented warming in the 2020s, not only at the surface but also in the subsurface. These subsurface temperature anomalies are likely linked to changes in ocean circulation especially in the western NP. In this section, we investigate the changes in ocean circulation in the western NP and their relationship to the SST and OHC changes.

Figure **10** compares the zonal and meridional current transport changes between 2020-2024 and 2010-2019 in the 0-300 m depth range with the SST and 0-300 m OHC changes. The northward transport anomalies are evident near the Japan coast accompanied by southward anomalies to the east (**Fig. 10c**). These northward and southward transport anomalies, as well as time-mean transports in 2020-2024 (**Fig. 10d**), sandwich the high SST and OHC anomalies between them (**Figs. 10ab**). These results suggest that the temperature advection from the Kuroshio provide the warm water anomalies, consistent with the evidence of the Kuroshio water intrusion identified by in-situ observation in this area in 2022 (Kawai et al., 2024) and in 2024 (Sugimoto et al., 2025). The features shown in Fig. 10c,d suggest that the intrusion of Kuroshio water occurs due to the northward extension of the Kuroshio itself up to 40°N, and that Kuroshio water is further transported by eddies detached from the Kuroshio up to 42°N. This interpretation is consistent with a visual inspection of SSH in each season and each year in this area (not shown).

The transport shows zonally extended eastward anomalies between 35°N and 37°N and westward anomalies between 33°N and 35°N between 150° and 170°E, indicating a northward migration of the Kuroshio Extension. This northward shift is associated with warm OHC anomalies and is also apparent in satellite-derived SSH data (not shown). To assess the magnitude of the meridional migration of the Kuroshio Extension, the meridional profiles of 0–300 m zonal transport between 155°E and 165°E are plotted for each decade (**Fig. 10e**). For this estimation, the zonal velocities from ORAS5, available only since 1975, are remapped onto a 0.25° latitude-longitude grid. The zonally averaged meridional profiles of 0–300 m transport in each decade clearly indicate a significant northward shift of the Kuroshio Extension in 2020-2024, with a difference of approximately 1.3° in latitude from the 2010s. Consequently, epochal differences in transport, characterized by the loop-like northward intrusion of the Kuroshio water reaching 42°N and the northward migration of the Kuroshio Extension, are closely linked to SST and OHC anomalies.

Although SST and OHC anomalies are prominent in the subarctic front region, transport anomalies there are much smaller than those in the Kuroshio Extension. Further studies are needed to understand the causes of SST and OHC warming in this region.

To highlight some notable changes that are challenging to discern in **Fig. 10c**, which has been adjusted to enhance visibility of the large variations in the Kuroshio Extension, **Fig. 11** shows the 0–300 m transport volume in the East China Sea and the western subarctic North Pacific. The northeastward flowing Kuroshio current in the East China Sea appears weakened, as shown by opposing southwestward anomalies. Similarly, the southwestward flowing Oyashio along the Kuril Islands is weakened. The weakening of the Kuroshio in the East China Sea was also reported for the period from 1993-2013 (Wang et al., 2016). Unlike the northward intrusion of the Kuroshio near Japan coast and the northward shift of the Kuroshio Extension, which show corresponding changes in OI-SST, no significant SST changes accompany the observed variations in the Kuroshio in the East China Sea or in the Oyashio along the Kuril Islands in Fig. 2. Therefore, further research is necessary to determine whether these current changes found in ORAS5 are indeed occurring.

3.4 Wind forcings

Figure 12 shows the WB transport estimated by Sverdrup theory in combination with EOF analysis, along with the climatology of the estimated WB transport. The climatological transport reaches a maximum value of approximately 40 Sv around 30°N and decreases both northward and southward from there. To the north, it crosses zero between 40°N and 45°N, reaching about -30 Sv at the northern boundary of the calculation region. The EOF1 pattern of Sverdrup transport shows opposite signs between the north and south, indicating that this mode generally acts to strengthen or weaken both the subtropical and subpolar circulations, though the usefulness of estimation of WB transport based on Sverdrup framework may have difficulties for subpolar gyre as described in section 2. The zero-crossing of EOF1 occurs around 34°N, nearly 10° south of the climatological zero-crossing latitude. Therefore, when this mode strengthens the subtropical and subpolar circulations, it simultaneously tends to shift the circulation boundary southward; conversely, when it weakens the circulations, it tends to shift the boundary northward.

The time series for the first EOF mode (the first principal component (PC1)) reveals pronounced anomalies in recent years. **Figure 12b** shows that PC1 remains generally positive after 2018, with the 5-year running mean reaching its highest value on record by the end of the period (averaged from July 2019 to June 2024). The positive PC1, combined with the spatial pattern of EOF1, suggests that this mode tends to weaken both the subtropical and subpolar gyres while shifting the gyre boundary northward in the 2020s. The northward shift of the gyre boundary is consistent with the northward migration of the Kuroshio Extension shown in **Fig. 6**, and the decline of the subtropical gyre is consistent with analysis by Japan Meteorological Agency (JMA), which publishes online report[5] for the transport of the Kuroshio, based on 137E repeat observation line data, and the results indicate the overall weakening from 2000 to 2023.

The temporal variability of the first EOF mode of the Sverdrup transport is closely related to the strength of the Aleutian Low, represented by the North Pacific Index (NPI), area-averaged SLP over 30-65N, 160E-140W (Trenberth and Hurrell, 1994) in **Fig. 12b**. The correlation coefficient between the two is 0.82 for annual raw data and 0.76 for data with a five-year moving average. However, the Aleutian Low strength exhibits a more abrupt sign reversal in the 1970s—a characteristic known as the climate regime shift (Mantua et al., 1997; Minobe, 1997, 1999). A reversal of this change occurred in the mid-2000s, during which the weakening of the Aleutian Low was also sharper than the change in PC1. Relatedly, since 2018, positive anomalies have dominated in both time series, with PC1 showing a more pronounced deviation compared to the NPI relative to pre-2000 values. Thus, while PC1 and the NPI are closely related, the regime shift-like abrupt changes observed in the NPI are less evident in PC1. This difference is related to the fact that the PC1 deviations since 2018 are particularly large compared to those after 1970. The wind-anomalies, however, were not likely to be outstandingly unprecedented as shown in the anomalies with similar magnitudes in the 1960s, contrasting exceptional warming in SST and OHCs. Therefore, the abnormal conditions in the 2020s may be related to the wind-field change but cannot be fully explained by them.

It is of interest to examine further the relationship between Sverdrup transport PC1 and the meridional migration of the current system. The gyre boundary mentioned above is used conceptually; however, no clear gyre boundary is evident in the western NP. To evaluate the meridional shift of the current system, the mean latitude of 0–300 m transport is estimated using the following equation:

---

[5] https://www.data.jma.go.jp/kaiyou/data/shindan/b_2/kuroshio_stream/kuroshio_stream.html (access 2025/2/12)

$$y_T(t) = \frac{\int_{x_W}^{x_E}\int_{y_S}^{y_N} yU(x,y,t)dy\,dx}{\int_{x_W}^{x_E}\int_{y_S}^{y_N} U(x,y,t)dy\,dx} \qquad (3)$$

where y_T is the mean transport latitude, U is the zonal transport integrated over 0–300 m, t is the time, y is the latitude, x is the longitude. This metric is robustly calculated even when the Kuroshio Extension exhibits a double-peak structure, as seen in the 1975–79 profile in Fig. 10e. The estimation is performed over the region 30°–40°N, 155°–165°E. It should be noted that this metric is experimental, designed with an emphasis on computational robustness.

As shown in **Fig. 13a**, Sverdrup transport PC1 and the observed mean transport latitude exhibit a strong correlation with a two-year lag (PC1 leading). The lag correlation coefficient is 0.7 when applying a five-year running mean. This time lag is generally consistent with previous studies (e.g. Qiu et al., 2023).

To further quantify this relationship, the meridional migration of the gyre boundary is estimated by combining information from the climatological Sverdrup transport and interannual variations in Sverdrup EOF1. Around the latitude where the climatological Sverdrup transport is zero, its gradient is approximately ±20 Sv per 10° of latitude, while EOF1 has a magnitude of about 5 Sv at this latitude. Consequently, a one-standard-deviation change in PC1 corresponds to an estimated meridional shift of 1.25° (1.25 = 5 Sv / (40 Sv/10°)).

If this estimation holds in reality, the estimated and observed latitude anomalies should have similar magnitudes. However, the regression coefficient between the estimated and observed latitude anomalies is 0.5 (**Fig. 13b**), indicating that the estimation overpredicts the actual shift by a factor of two. Given the limitations of Sverdrup theory discussed in Section 2 and the experimental nature of the metric of mean transport latitude, a factor-of-two discrepancy may still be reasonable, as it suggests that Sverdrup theory provides useful insight despite its simplifications.

4. Summary, Discussion and Conclusions

4.1 Summary

The present paper investigates the recent exceptional conditions in NP. The anomalous conditions started in the late 2010s and intensified rapidly to the present (February 2025). The signatures suggest that the anomalous conditions in the 2020s developed separately in the western and eastern North Pacific—beginning in the west, associated with changes in the Kuroshio and Oyashio currents, and emerging in the east with a lag of one to two years (**Fig. 2**). The SST anomalies are exceptionally strong, reaching 6°C for anomalies in the K-O area relative to the previous 30-years 1990-2019 (**Fig. 1**). Subsurface temperature also exhibits high anomalies (**Fig. 3**), with 28% share of 0-300 OHC warming in NP for the global ocean (**Table 1**). The exceptional heat is linked to MHWs in the North Pacific. In particular, severe and extreme MHWs in this basin exhibited the largest area-day fraction among the world's oceans (**Fig. 7**), with the majority occurring near Japan (**Fig. 9**), including ultra MHWs. In the 2020s, the Kuroshio water strongly intruded to about 42°N along the Japan coast accompanied by southward return flow to just to the east of the intruding northward flow, forming a loop-like shape (**Fig. 10**). Also, the Kuroshio Extension shifted to the north (**Fig. 10**). The anomalous condition in the North Pacific is likely to be related to the wind field change, which can act to weaken the subtropical gyre with shifting subtropical/subpolar gyre boundary northward as suggested from Sverdrup theory (**Figs. 12, 13**).

Some of the changes reported in this paper are consistent with recent publications, reinforcing their findings. Northward shifts in the Kuroshio current up to 2021 were documented by Kawakami et al. (2023), while Kawai et al. (2023) reported on OHC increase across the North Pacific up to 2020. The pronounced SST warming in the North Pacific was also examined by Hu et al. (2024). Sugimoto et al. (2025) reported ship observation results across a warm core eddy off Tohoku in May 2024. The present study places particular emphasis on analyzing the relationships among SST, OHC, and ocean currents, offering a closer look at the interactions driving these changes. Additionally, by incorporating recent data through 2023–24, this study underscores the significant role of the NP in contributing to global ocean heat content changes.

Since the exceptional heat in the K-O region and in the NP basin suggests that a substantial body of future studies are needed. In the following subsections, some of those opportunities are discussed.

4.2 Discussion, future opportunities

a. Can state-of-art OGCMs simulate exceptional conditions in NP in recent years?

To understand the mechanisms behind the exceptional conditions of the 2020s, numerical model simulations and experiments are highly desirable. A key first step in this direction is to assess whether the exceptional 2020s conditions can be reasonably simulated by state-of-art ocean models forced by observed boundary conditions. Recently, Kawakami et al., (2023) conducted a simulation using an eddy-resolving regional ocean model nested within a coarse-resolution global model for the period 1960–2021. Their experiment largely follows the Ocean Model Intercomparison Project Phase 2 (OMIP2) protocol (Tsujino et al., 2020) but extends the simulation period to 2021, three years beyond the standard OMIP2 endpoint of 2018.

Results from Kawakami et al. (2023) indicate a northward shift in the Kuroshio Extension latitude, along with decadal variability that aligns qualitatively with observed patterns, including consistent decadal fluctuations. However, the model somewhat underestimated the unusually rapid northward migration of the Kuroshio Extension around 2020 (see their Fig. 2a and Fig. 7a). This raises the question of whether current state-of-the-art ocean models can adequately capture the exceptional conditions observed in the 2020s. Therefore, it is essential to compare results from other eddy-resolving ocean models to determine if the current generation of ocean models can reliably simulate these exceptional conditions in the K-O region. If OGCMs are able to replicate the 2020s conditions reasonably, further experiments should be conducted to understand the underlying mechanisms. Also, heat budget analyses should be conducted to determine where the heat came from to the NP.

b. Are the exceptional conditions driven by anthropogenic influences?

An important question is whether the exceptional North Pacific conditions in the 2020s are a harbinger of global warming. For the eastern NP, Barkhordarian et al., (2022) suggested that the long-term “warming pool” in the northeastern North Pacific in the 2010s and 2020s driven by the anthropogenic increase in greenhouse gases (GHGs), combined with the recent decrease in anthropogenic aerosols. For the western NP, it has been reported that the Kuroshio Extension shows a northward shift in observational data analyses over the past few decades. Wu et al. (2021) reported a northward trend of approximately 0.23° per decade from 1979 to 2018, while Kawakami et al. (2023) reported a trend of 0.66° per decade from 1993 to 2021. As the ocean absorbs 89% of the excess heat taken up by the Earth's climate system due to global warming (Von Schuckmann et al., 2023), and the Kuroshio current serves as a key pathway for the global transport of oceanic heat, a portion of the heat gained by the ocean under global warming may be transported to the North Pacific through the Kuroshio and subsequently released into the atmosphere.

However, projected migration of the Kuroshio Extension based on high-resolution ocean downscaling of CMIP5 climate models is estimated to range from 0.26° to 0.89° for the end of the 21st century in the RCP8.5 scenario (Nishikawa et al., 2020), smaller than the observed shift in the last few decades. The weak meridional migration is consistent with the moderate migration signatures reported by Terada and Minobe (2018), who analyzed 35 CMIP5 models. Therefore, if the climate models are reliable, it is likely that a substantial portion of the observed northward shift in the Kuroshio Extension is attributable to natural variability.

On the other hand, the reliability of climate models is under debate about the climate change pattern in the tropics and its teleconnection. Climate models generally project El Nino-like warming patterns in the tropics, but a La Niña-like trend is observed during the satellite era, which could be influenced by human activities (Watanabe et al., 2024). In association with a modeled El Niño-like warming pattern, the Aleutian Low may intensify under future global warming (Gan et al., 2017), in contrast to its weakening over the past three decades (**Fig. 12b**). Furthermore, if the observed La Niña-like trend is natural variability, the recent weakening of the Aleutian Low may also result from natural variability within the tropical Pacific (Capotondi et al., 2023). Therefore, further studies are needed to conclude the contribution of natural and anthropogenic origin of the observed northward Kuroshio Extension migration.

c. What is likely to occur in the coming years?

Since the North Pacific is currently storing an unusual amount of heat (Fig. 3), understanding what will happen to this heat in the coming years is crucial. It will be highly interesting to examine the predictions produced by various forecast models on this matter. Multi-year predictions are conducted within the framework of CMIP6 under the Decadal Climate Prediction Project (Boer et al., 2016), and the World Meteorological Organization, through The Lead Centre for Annual-to-Decadal Climate Prediction[6], collects data from contributing centers worldwide to summarize prediction information. Although the multi-annual predictability of the NP is generally smaller than those compared to the Atlantic (Boer et al., 2016), prediction systems that utilized high-resolution models exhibited that the Kuroshio Extension can be predicted with multi-annual lead time (Kido et al., 2023; Kim et al., 2023).

While numerical forecast simulations and analysis of their results should be addressed in a separate paper, the data examined in this study has provided intriguing insights about the near future, which I would like to share. **Figure 14** shows an x-t diagram of SSH within three 5-degree north-south bands based on satellite observations. Following changes in atmospheric circulation around 2018 in **Fig. 12b**, positive anomalies were triggered in the eastern NP and have since been propagating westward. The propagating positive SSH anomalies are in the central-eastern NP at the end of the record (November 2024). If this propagation continues, it is expected that the western NP will experience the effects of these positive anomalies over the coming years to possibly a decade. However, it is not certain that these positive anomalies will reach the western NP. Qiu (2003) suggests that the westward propagation of SSH north of the Kuroshio Extension may not penetrate into the western NP.

d. Assessments of impacts on marine ecosystem

It is widely recognized that global warming and marine heatwaves have had substantial impacts on marine ecosystems (Cavole et al., 2016; Miyama et al., 2021; Yati et al., 2020). The magnitude of North Pacific heat and MHWs in recent years has exceeded past levels across many regions (Figs. 1 and 9). Consequently, wide-ranging effects on marine ecosystems are expected. To fully understand the extent of these impacts, international collaboration is essential. Also, investigations about forecasting impacts on marine ecosystems should be explored (see Minobe et al. (2022) and references therein).

[6] https://hadleyserver.metoffice.gov.uk/wmolc/ (access, Oct 31st, 2024)

4.3 Conclusions

The North Pacific has exhibited exceptional heat conditions in recent years, affecting both its western and eastern regions. The significant increase in OHC highlights the North Pacific's importance in ocean heat absorption and distribution under global warming. These anomalous conditions are likely related to the weakening of the Aleutian Low and associated atmospheric circulation changes, but understanding of mechanisms is still limited. Numerous research efforts are needed in the coming years, including understanding of mechanisms, continued vigilance regarding the ongoing extreme anomalies, improved predictions, and assessments of impacts on marine ecosystems.

Data Availability

Data are available from the following sites:

OI-SST, https://psl.noaa.gov/data/gridded/data.noaa.oisst.v2.html;

ERA5, https://www.ecmwf.int/en/forecasts/dataset/ecmwf-reanalysis-v5;

ORAS5, https://www.ecmwf.int/en/elibrary/80763-ocean5-ecmwf-ocean-reanalysis-system-and-its-real-time-analysis-component;

Grid-cell information of ORAS5, https://icdc.cen.uni-hamburg.de/thredds/catalog/ftpthredds/EASYInit/oras5/ORCA025/mesh/catalog.html;

EN4 temperature and salinity data, https://www.metoffice.gov.uk/hadobs/en4/

JMA temperature and salinity data, https://climate.mri-jma.go.jp/pub/ocean/ts/v7.3.1/

IAP OHC data, http://www.ocean.iap.ac.cn/

Satellite SSH,
https://data.marine.copernicus.eu/product/SEALEVEL_GLO_PHY_CLIMATE_L4_MY_008_057/
for two-satellite delayed time data, and

https://data.marine.copernicus.eu/product/SEALEVEL_GLO_PHY_L4_NRT_008_046

for all-satellite near-real-time data.

Code Availability

All codes are available upon reasonable request to the corresponding author.

Acknowledgement

This work was supported by the Ministry of Education, Culture, Sports, Science and Technology (MEXT) of Japan, Grant-in-Aid for Scientific Research on Innovative Areas (19H05704, 24H01502). The author thanks two anonymous reviewers for their constructive comments.

Conflict of Interest

The authors declare that they have no known financial or non-financial competing interests that could have appeared to influence the work reported in this paper.

References

Amaya, D. J., Miller, A. J., Xie, S.-P., & Kosaka, Y. (2020). Physical drivers of the summer 2019 North Pacific marine heatwave. Nature Communications, 11(1), 1903. https://doi.org/10.1038/s41467-020-15820-w

Andres, M., Kwon, Y.-O., & Yang, J. (2011). Observations of the Kuroshio's barotropic and baroclinic responses to basin-wide wind forcing. Journal of Geophysical Research, 116(C4), C04011. https://doi.org/10.1029/2010JC006863

Barkhordarian, A., Nielsen, D. M., & Baehr, J. (2022). Recent marine heatwaves in the North Pacific warming pool can be attributed to rising atmospheric levels of greenhouse gases. *Communications Earth & Environment*, *3*(1), 131. https://doi.org/10.1038/s43247-022-00461-2

Boer, G. J., Smith, D. M., Cassou, C., Doblas-Reyes, F., Danabasoglu, G., Kirtman, B., Kushnir, Y., Kimoto, M., Meehl, G. A., Msadek, R., Mueller, W. A., Taylor, K. E., Zwiers, F., Rixen, M., Ruprich-Robert, Y., & Eade, R. (2016). The Decadal Climate Prediction Project (DCPP) contribution to CMIP6. Geoscientific Model Development, 9(10), 3751–3777. https://doi.org/10.5194/gmd-9-3751-2016

Capotondi, A., McGregor, S., McPhaden, M. J., Cravatte, S., Holbrook, N. J., Imada, Y., Sanchez, S. C., Sprintall, J., Stuecker, M. F., Ummenhofer, C. C., Zeller, M., Farneti, R., Graffino, G., Hu, S., Karnauskas, K. B., Kosaka, Y., Kucharski, F., Mayer, M., Qiu, B., … Xu, T. (2023). Mechanisms of tropical Pacific decadal variability. Nature Reviews Earth & Environment, 4(11), 754–769. https://doi.org/10.1038/s43017-023-00486-x

Capotondi, A., Rodrigues, R. R., Sen Gupta, A., Benthuysen, J. A., Deser, C., Frölicher, T. L., Lovenduski, N. S., Amaya, D. J., Le Grix, N., Xu, T., Hermes, J., Holbrook, N. J., Martinez-Villalobos, C., Masina, S., Roxy, M. K., Schaeffer, A., Schlegel, R. W., Smith, K. E., & Wang, C. (2024). A global overview of marine heatwaves in a changing climate. Communications Earth & Environment, 5(1), 701. https://doi.org/10.1038/s43247-024-01806-9

Cavole, L., Demko, A., Diner, R., Giddings, A., Koester, I., Scripps Institution of Oceanography, Pagniello, C., Paulsen, M.-L., Ramirez-Valdez, A., Schwenck, S., Yen, N., Zill, M., & Franks, P. (2016). Biological Impacts of the 2013–2015 Warm-Water Anomaly in the Northeast Pacific:

Winners, Losers, and the Future. Oceanography, 29(2). https://doi.org/10.5670/oceanog.2016.32

Ceballos, L. I., Di Lorenzo, E., Hoyos, C. D., Schneider, N., & Taguchi, B. (2009). North Pacific Gyre Oscillation Synchronizes Climate Fluctuations in the Eastern and Western Boundary Systems*. Journal of Climate, 22(19), 5163–5174. https://doi.org/10.1175/2009JCLI2848.1

Cheng, L., Abraham, J., Trenberth, K. E., Boyer, T., Mann, M. E., Zhu, J., Wang, F., Yu, F., Locarnini, R., Fasullo, J., Zheng, F., Li, Y., Zhang, B., Wan, L., Chen, X., Wang, D., Feng, L., Song, X., Liu, Y., … Lu, Y. (2024). New Record Ocean Temperatures and Related Climate Indicators in 2023. Advances in Atmospheric Sciences. https://doi.org/10.1007/s00376-024-3378-5

Cheng, L., Pan, Y., Tan, Z., Zheng, H., Zhu, Y., Wei, W., Du, J., Yuan, H., Li, G., Ye, H., Gouretski, V., Li, Y., Trenberth, K. E., Abraham, J., Jin, Y., Reseghetti, F., Lin, X., Zhang, B., Chen, G., … Zhu, J. (2024). IAPv4 ocean temperature and ocean heat content gridded dataset. Earth System Science Data, 16(8), 3517–3546. https://doi.org/10.5194/essd-16-3517-2024

Frölicher, T. L., Fischer, E. M., & Gruber, N. (2018). Marine heatwaves under global warming. *Nature*, *560*(7718), 360–364. https://doi.org/10.1038/s41586-018-0383-9

Gan B., Wu L., Jia F., Li S., Cai W., Nakamura H., Alexander M. A., & Miller A. J. (2017). On the Response of the Aleutian Low to Greenhouse Warming. Journal of Climate, https://doi.org/10.1175/JCLI-D-15-0789.1

Gelaro, R., McCarty, W., Suárez, M. J., Todling, R., Molod, A., Takacs, L., Randles, C. A., Darmenov, A., Bosilovich, M. G., Reichle, R., Wargan, K., Coy, L., Cullather, R., Draper, C., Akella, S., Buchard, V., Conaty, A., Da Silva, A. M., Gu, W., … Zhao, B. (2017). The Modern-Era Retrospective Analysis for Research and Applications, Version 2 (MERRA-2). Journal of Climate, 30(14), 5419–5454. https://doi.org/10.1175/JCLI-D-16-0758.1

Goessling, H. F., Rackow, T., & Jung, T. (2025). Recent global temperature surge intensified by record-low planetary albedo. Science, 387(6729), 68–73. https://doi.org/10.1126/science.adq7280

Good, S. A., Martin, M. J., & Rayner, N. A. (2013). EN4: Quality controlled ocean temperature and salinity profiles and monthly objective analyses with uncertainty estimates. Journal of Geophysical Research: Oceans, 118(12), 6704–6716. https://doi.org/10.1002/2013JC009067

Hersbach, H., Bell, B., Berrisford, P., Hirahara, S., Horányi, A., Muñoz-Sabater, J., Nicolas, J., Peubey, C., Radu, R., Schepers, D., Simmons, A., Soci, C., Abdalla, S., Abellan, X., Balsamo, G., Bechtold, P., Biavati, G., Bidlot, J., Bonavita, M., … Thépaut, J. (2020). The ERA5 global reanalysis. Quarterly Journal of the Royal Meteorological Society, 146(730), 1999–2049. https://doi.org/10.1002/qj.3803

Hobday, A. J., Alexander, L. V., Perkins, S. E., Smale, D. A., Straub, S. C., Oliver, E. C. J., Benthuysen, J. A., Burrows, M. T., Donat, M. G., Feng, M., Holbrook, N. J., Moore, P. J., Scannell, H. A., Sen Gupta, A., & Wernberg, T. (2016). A hierarchical approach to defining marine heatwaves. Progress in Oceanography, 141, 227–238. https://doi.org/10.1016/j.pocean.2015.12.014

Hobday, A., Oliver, E., Sen Gupta, A., Benthuysen, J., Burrows, M., Donat, M., Holbrook, N., Moore, P., Thomsen, M., Wernberg, T., & Smale, D. (2018). Categorizing and Naming Marine Heatwaves. Oceanography, 31(2). https://doi.org/10.5670/oceanog.2018.205

Hu, Z.-Z., McPhaden, M. J., Huang, B., Zhu, J., & Liu, Y. (2024). Accelerated warming in the North Pacific since 2013. Nature Climate Change, 14(9), 929–931. https://doi.org/10.1038/s41558-024-02088-x

Huang, B., Liu, C., Banzon, V., Freeman, E., Graham, G., Hankins, B., Smith, T., & Zhang, H.-M. (2021). Improvements of the Daily Optimum Interpolation Sea Surface Temperature (DOISST) Version 2.1. Journal of Climate, 34(8), 2923–2939. https://doi.org/10.1175/JCLI-D-20-0166.1

Ishii, M., Fukuda, Y., Hirahara, S., Yasui, S., Suzuki, T., & Sato, K. (2017). Accuracy of Global Upper Ocean Heat Content Estimation Expected from Present Observational Data Sets. SOLA, 13(0), 163–167. https://doi.org/10.2151/sola.2017-030

Kawai, Y., Nagano, A., Hasegawa, T., Tomita, H., & Tani, M. (2023). Decadal changes in the basin-wide heat budget of the mid-latitude North Pacific Ocean. Journal of Oceanography, 79(2), 91–108. https://doi.org/10.1007/s10872-022-00667-0

Kawai, Y., Oka, E., Sato, K., Hosoda, S., & Kido, S. (2024). Marine heatwave in the Oyashio region in 2022/23 and its impact on subsurface dissolved oxygen. Journal of Oceanography. https://doi.org/10.1007/s10872-024-00731-x

Kawakami, Y., Kojima, A., Murakami, K., Nakano, T., & Sugimoto, S. (2022). Temporal variations of net Kuroshio transport based on a repeated hydrographic section along 137°E. Climate Dynamics, 59(5–6), 1703–1713. https://doi.org/10.1007/s00382-021-06061-8

Kawakami, Y., Nakano, H., Urakawa, L. S., Toyoda, T., Aoki, K., Hirose, N., & Usui, N. (2024). Temporal changes of the Oyashio water distribution east of Japan under the changing climate: Development of an objective evaluation method and its application. Journal of Oceanography. https://doi.org/10.1007/s10872-024-00727-7

Kawakami, Y., Nakano, H., Urakawa, L. S., Toyoda, T., Aoki, K., & Usui, N. (2023). Northward shift of the Kuroshio Extension during 1993–2021. Scientific Reports, 13(1), 16223. https://doi.org/10.1038/s41598-023-43009-w

Kida, S., Mitsudera, H., Aoki, S., Guo, X., Ito, S., Kobashi, F., Komori, N., Kubokawa, A., Miyama, T., Morie, R., Nakamura, H., Nakamura, T., Nakano, H., Nishigaki, H., Nonaka, M., Sasaki, H., Sasaki, Y. N., Suga, T., Sugimoto, S., … Usui, N. (2015). Oceanic fronts and jets around Japan: A review. Journal of Oceanography, 71(5), 469–497. https://doi.org/10.1007/s10872-015-0283-7

Kido, S., Nonaka, M., & Miyazawa, Y. (2023). Skillful Multiyear Prediction of the Kuroshio and Gulf Stream Jets and Eddy Activity. Geophysical Research Letters, 50(15), e2023GL103705. https://doi.org/10.1029/2023GL103705

Kim, W. M., Yeager, S. G., Danabasoglu, G., & Chang, P. (2023). Exceptional multi-year prediction skill of the Kuroshio Extension in the CESM high-resolution decadal prediction system. Npj Climate and Atmospheric Science, 6(1), 118. https://doi.org/10.1038/s41612-023-00444-w

Kosaka, Y., Kobayashi, S., Harada, Y., Kobayashi, C., Naoe, H., Yoshimoto, K., Harada, M., Goto, N., Chiba, J., Miyaoka, K., Sekiguchi, R., Deushi, M., Kamahori, H., Nakaegawa, T., Tanaka, T. Y., Tokuhiro, T., Sato, Y., Matsushita, Y., & Onogi, K. (2024). The JRA-3Q Reanalysis. Journal of the Meteorological Society of Japan. Ser. II, 102(1), 49–109. https://doi.org/10.2151/jmsj.2024-004

Kuroda, H., & Setou, T. (2021). Extensive Marine Heatwaves at the Sea Surface in the Northwestern Pacific Ocean in Summer 2021. Remote Sensing, 13(19), 3989. https://doi.org/10.3390/rs13193989

Larson, J. G., Thompson, D. W. J., & Hurrell, J. W. (2024). Signature of the western boundary currents in local climate variability. Nature, 634(8035), 862–867. https://doi.org/10.1038/s41586-024-08019-2

Mantua, N. J., Hare, S. R., Zhang, Y., Wallace, J. M., & Francis, R. C. (1997). A Pacific Interdecadal Climate Oscillation with Impacts on Salmon Production. Bulletin of the American Meteorological Society, 78(6), 1069–1079. https://doi.org/10.1175/1520-0477(1997)078<1069:APICOW>2.0.CO;2

Minobe, S. (1997). A 50–70 year climatic oscillation over the North Pacific and North America. Geophysical Research Letters, 24(6), 683–686. https://doi.org/10.1029/97GL00504

Minobe, S. (1999). Resonance in bidecadal and pentadecadal climate oscillations over the North Pacific: Role in climatic regime shifts. Geophysical Research Letters, 26(7), 855–858. https://doi.org/10.1029/1999GL900119

Minobe, S., Capotondi, A., Jacox, M. G., Nonaka, M., & Rykaczewski, R. R. (2022). Toward Regional Marine Ecological Forecasting Using Global Climate Model Predictions From Subseasonal to Decadal Timescales: Bottlenecks and Recommendations. Frontiers in Marine Science, 9, 855965. https://doi.org/10.3389/fmars.2022.855965

Minobe, S., & Maeda, A. (2005). A 1° monthly gridded sea-surface temperature dataset compiled from ICOADS from 1850 to 2002 and Northern Hemisphere frontal variability. International Journal of Climatology, 25(7), 881–894. https://doi.org/10.1002/joc.1170

Minobe, S., Behrens, E., Findell, K. L., Loeb, N. G., Meyssignac, B., & Sutton, R. (2025). Global and Regional Drivers for Exceptional Climate Extremes in 2023-2024: Beyond the New Normal. *npj Clim Atmos Sci* **8**, 138. https://doi.org/10.1038/s41612-025-00996-z.

Miyama, T., Minobe, S., & Goto, H. (2021). Marine Heatwave of Sea Surface Temperature of the Oyashio Region in Summer in 2010–2016. Frontiers in Marine Science, 7, 576240. https://doi.org/10.3389/fmars.2020.576240

Nakamura, H. (1998). Simple Model Prediction of Horizontal Temperature Fields in the Subtropical–Subpolar System Caused by Sudden Change in Wind Stress Curl. Journal of Physical Oceanography, 28(8), 1578–1597. https://doi.org/10.1175/1520-0485(1998)028<1578:SMPOHT>2.0.CO;2

Nakamura, H., Lin, G., & Yamagata, T. (1997). Decadal Climate Variability in the North Pacific during the Recent Decades. Bulletin of the American Meteorological Society, 78(10), 2215–2225. https://doi.org/10.1175/1520-0477(1997)078<2215:DCVITN>2.0.CO;2

Newman, M., Alexander, M. A., Ault, T. R., Cobb, K. M., Deser, C., Di Lorenzo, E., Mantua, N. J., Miller, A. J., Minobe, S., Nakamura, H., Schneider, N., Vimont, D. J., Phillips, A. S., Scott, J. D., & Smith, C. A. (2016). The Pacific Decadal Oscillation, Revisited. *Journal of Climate*, *29*(12), 4399–4427. https://doi.org/10.1175/JCLI-D-15-0508.1

Nishihira, G., & Sugimoto, S. (2024). Record-Breaking Marine Heatwave over the Central North Pacific in 2021 Summer: Its Formation Associated with Loss of Central Mode Water. Journal of Physical Oceanography, 54(11), 2361–2372. https://doi.org/10.1175/JPO-D-24-0021.1

Nishikawa, H., Nishikawa, S., Ishizaki, H., Wakamatsu, T., & Ishikawa, Y. (2020). Detection of the Oyashio and Kuroshio fronts under the projected climate change in the 21st century. Progress in Earth and Planetary Science, 7(1), Article 1. https://doi.org/10.1186/s40645-020-00342-2

Oka, E., Sugimoto, S., Kobashi, F., Nishikawa, H., Kanada, S., Nasuno, T., Kawamura, R., & Nonaka, M. (2023). Subtropical Mode Water south of Japan impacts typhoon intensity. Science Advances, 9(37), eadi2793. https://doi.org/10.1126/sciadv.adi2793

Qiu, B. (2003). Kuroshio Extension Variability and Forcing of the Pacific Decadal Oscillations: Responses and Potential Feedback. Journal of Physical Oceanography, 33(12), 2465–2482. https://doi.org/10.1175/1520-0485(2003)033<2465:KEVAFO>2.0.CO;2

Qiu, B., Chen, S., & Oka, E. (2023). Why Did the 2017 Kuroshio Large Meander Event Become the Longest in the Past 70 Years? Geophysical Research Letters, 50(10), e2023GL103548. https://doi.org/10.1029/2023GL103548

Sasaki, Y. N., & Ito, R. (2024). Impact of the Kuroshio large meander on local atmospheric circulation and precipitation in winter. Progress in Earth and Planetary Science, 11(1), 15. https://doi.org/10.1186/s40645-024-00620-3

Sasaki, Y. N., Minobe, S., & Schneider, N. (2013). Decadal Response of the Kuroshio Extension Jet to Rossby Waves: Observation and Thin-Jet Theory*. Journal of Physical Oceanography, 43(2), 442–456. https://doi.org/10.1175/JPO-D-12-096.1

Sasaki, Y. N., & Schneider, N. (2011). Decadal Shifts of the Kuroshio Extension Jet: Application of Thin-Jet Theory. Journal of Physical Oceanography, 41(5), 979–993. https://doi.org/10.1175/2010JPO4550.1

Sato, H., Takemura, K., Ito, A., Umeda, T., Maeda, S., Tanimoto, Y., Nonaka, M., & Nakamura, H. (2024). Impact of an unprecedented marine heatwave on extremely hot summer over Northern Japan in 2023. Scientific Reports, 14(1), 16100. https://doi.org/10.1038/s41598-024-65291-y

Sheng, J., Liu, C., Gu, Y., Li, P., Zhai, F., & Zhou, N. (2024). Anomalous North Pacific subtropical mode water volume and density decrease in a recent stable Kuroshio Extension period from Argo observations. Ocean Science, 20(3), 817–834. https://doi.org/10.5194/os-20-817-2024

Sugimoto, S., Qiu, B., & Schneider, N. (2021). Local Atmospheric Response to the Kuroshio Large Meander Path in Summer and Its Remote Influence on the Climate of Japan. Journal of Climate, 34(9), 3571–3589. https://doi.org/10.1175/JCLI-D-20-0387.1

Sugimoto S., A. Kojima, T. Sakamoto, Y,. Kawakami, and H. Nakano. (2025). Influence of extreme northward meandered Kuroshio Extension during 2023-2024 on ocean-atmosphere conditions in the Sanrik offshore region, Japan. *Journal of Oceanography*, https://doi.org/10.1007/s10872-025-00747-x

Taguchi, B., Xie, S.-P., Schneider, N., Nonaka, M., Sasaki, H., & Sasai, Y. (2007). Decadal Variability of the Kuroshio Extension: Observations and an Eddy-Resolving Model Hindcast*. Journal of Climate, 20(11), 2357–2377. https://doi.org/10.1175/JCLI4142.1

Terada, M., & Minobe, S. (2018). Projected sea level rise, gyre circulation and water mass formation in the western North Pacific: CMIP5 inter-model analysis. Climate Dynamics, 50(11–12), 4767–4782. https://doi.org/10.1007/s00382-017-3902-8

Trenberth, K. E., & Hurrell, J. W. (1994). Decadal atmosphere-ocean variations in the Pacific. Climate Dynamics, 9(6), 303–319. https://doi.org/10.1007/BF00204745

Tsujino, H., Urakawa, L. S., Griffies, S. M., Danabasoglu, G., Adcroft, A. J., Amaral, A. E., Arsouze, T., Bentsen, M., Bernardello, R., Böning, C. W., Bozec, A., Chassignet, E. P., Danilov, S., Dussin, R., Exarchou, E., Fogli, P. G., Fox-Kemper, B., Guo, C., Ilicak, M., … Yu, Z. (2020). Evaluation of global ocean–sea-ice model simulations based on the experimental protocols of the Ocean Model Intercomparison Project phase 2 (OMIP-2). Geoscientific Model Development, 13(8), 3643–3708. https://doi.org/10.5194/gmd-13-3643-2020

von Schuckmann, K., Minière, A., Gues, F., Cuesta-Valero, F. J., Kirchengast, G., Adusumilli, S., Straneo, F., Ablain, M., Allan, R. P., Barker, P. M., Beltrami, H., Blazquez, A., Boyer, T., Cheng, L., Church, J., Desbruyeres, D., Dolman, H., Domingues, C. M., García-García, A., … Zemp, M. (2023). Heat stored in the Earth system 1960–2020: Where does the energy go? Earth System Science Data, 15(4), 1675–1709. https://doi.org/10.5194/essd-15-1675-2023

Wang, Y., Wu, C., & Chao, S. (2016). Warming and weakening trends of the Kuroshio during 1993–2013. Geophysical Research Letters, 43(17), 9200–9207. https://doi.org/10.1002/2016GL069432

Watanabe, M., Kang, S. M., Collins, M., Hwang, Y.-T., McGregor, S., & Stuecker, M. F. (2024). Possible shift in controls of the tropical Pacific surface warming pattern. Nature, 630(8016), 315–324. https://doi.org/10.1038/s41586-024-07452-7

Wu, B., Lin, X., & Yu, L. (2021). Poleward Shift of the Kuroshio Extension Front and Its Impact on the North Pacific Subtropical Mode Water in the Recent Decades. Journal of Physical Oceanography, 51(2), 457–474. https://doi.org/10.1175/JPO-D-20-0088.1

Wunsch C., 2011; The decadal mean ocean circulation and Sverdrup balance. Journal of Marine Research, 69, 417–434 .

Yati, E., Minobe, S., Mantua, N., Ito, S., & Di Lorenzo, E. (2020). Marine Ecosystem Variations Over the North Pacific and Their Linkage to Large-Scale Climate Variability and Change. Frontiers in Marine Science, 7, 578165. https://doi.org/10.3389/fmars.2020.578165

Zuo, H., Balmaseda, M. A., Tietsche, S., Mogensen, K., & Mayer, M. (2019). The ECMWF operational ensemble reanalysis–analysis system for ocean and sea ice: A description of the system and assessment. Ocean Science, 15(3), 779–808. https://doi.org/10.5194/os-15-779-2019

Table and Figures

Table 1. Changes in Regional and Global 0-300 m Ocean Heat Content (OHC) between the 2010s (January 2010–December 2019) and the 2020s (January 2020–December 2024). The values represent the mean OHC change derived from four data products (ORAS5, JMA version 3.7.1, EN version 4.2, and IAP version 4), with the standard deviation across these products shown in parentheses.

Area name		Area share (%)	OHC Change (ZJ)	OHC Change Share (%)	OHC Change /Area (MJ/m^2)
Global		100.0	49.5 (2.5)	100.0 (0.0)	127 (18)
NH Mid-High Lats (20-90N)		26.7	24.1 (1.4)	48.7 (1.1)	240 (59)
	Western North Pacific (20-65N, 110E-175W)	5.8	7.8 (0.6)	15.8 (0.5)	346 (56)
	Eastern North Pacific (20-65N, 175W-100W)	5.7	5.8 (0.4)	11.8 (0.9)	265 (47)
	North Atlantic (20-65N, 100W-30E)	8.4	8.9 (0.9)	18.0 (1.4)	271 (50)
Tropics (20S-20N)		36.3	12.9 (1.2)	26.1 (1.3)	91 (9)
SH Mid-High Lats (90S-20S)		37.1	12.5 (0.6)	25.2 (1.5)	86 (8)

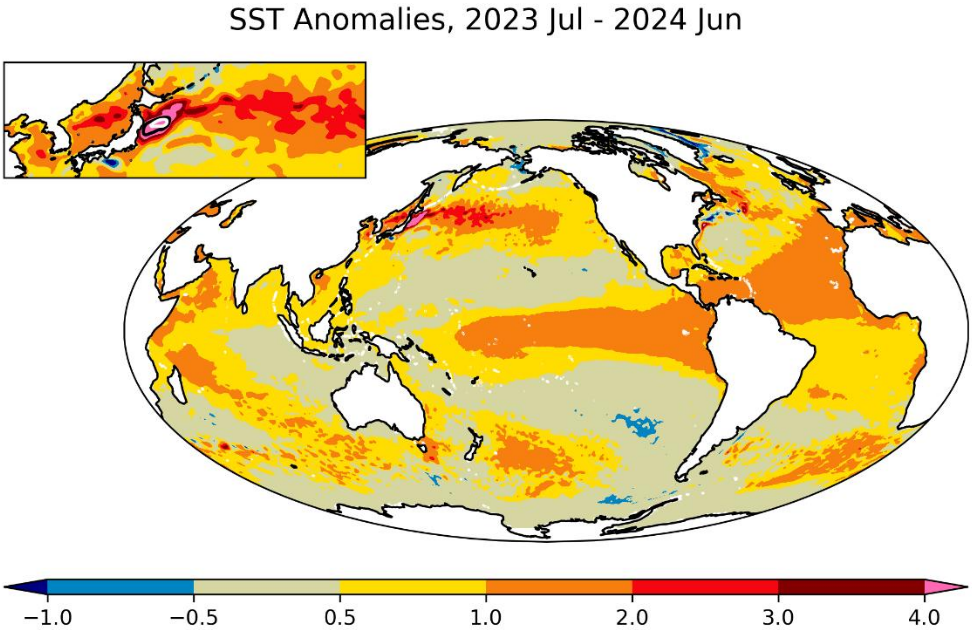

Fig. 1. SST anomalies averaged from July 2023 to June 2024, relative to 1990-2019 climatology. The black and white contours in the inset show 5 and 6°C anomalies.

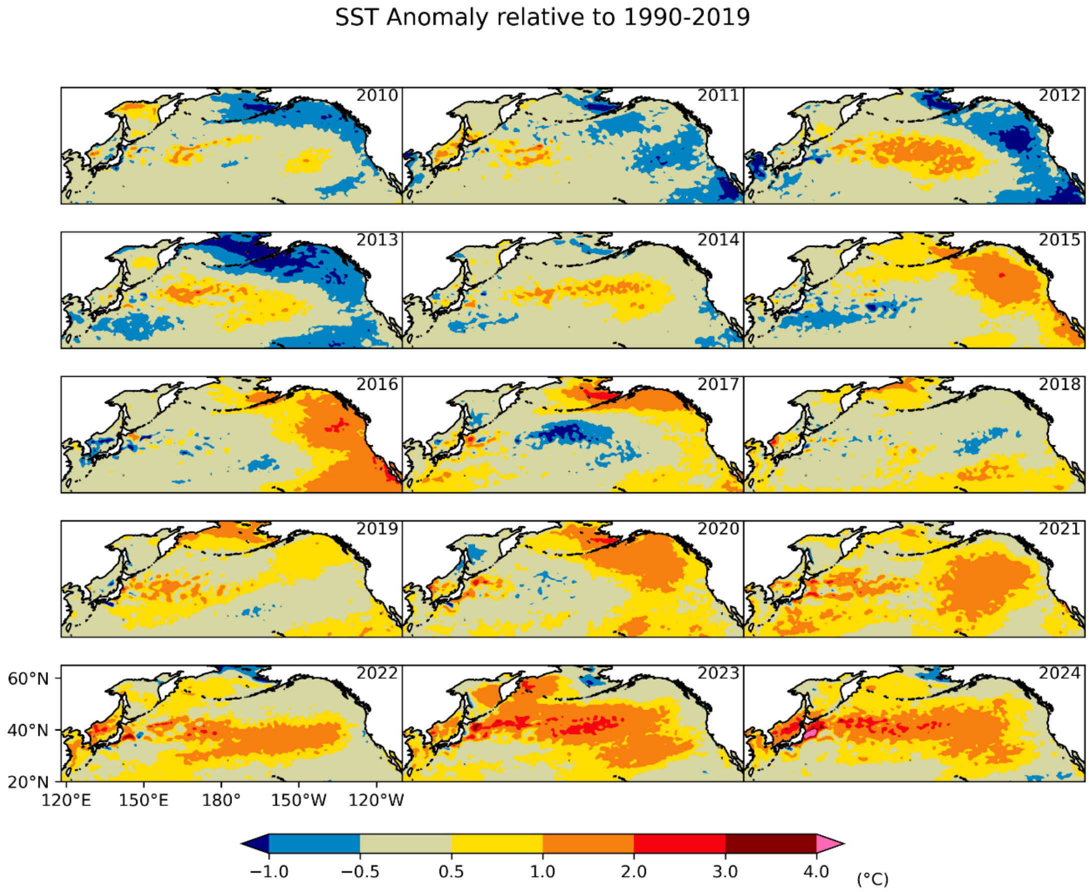

Fig. 2. Annual mean SST anomalies from 2010 to 2024, relative to 1990-2019 climatology. The anomalies are averaged from January to December in respective years.

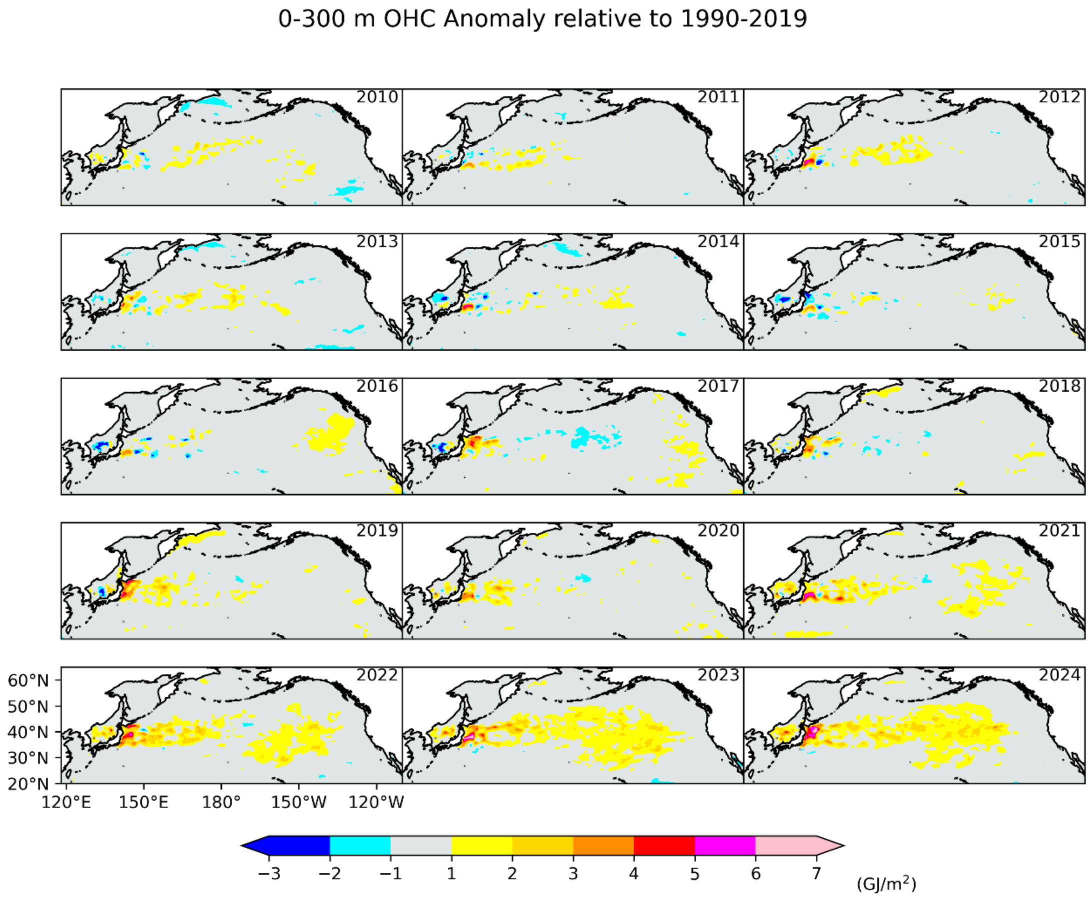

Fig 3. Same as Fig. 2, but for 0-300 m OHC per unit area.

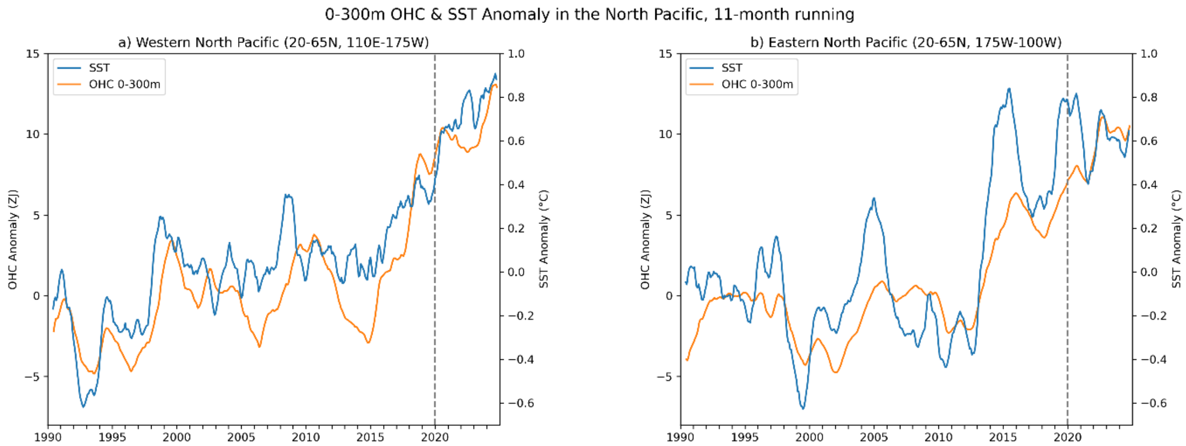

Fig. 4. Area averaged SST anomaly and area-integrated 0-300 m OHC anomaly over (a) the western North Pacific, and (b) eastern North Pacific. Anomalies are calculated relative to 1990-2019 and are smoothed by 11-month running mean. The vertical dashed line in each panel indicates 2020.

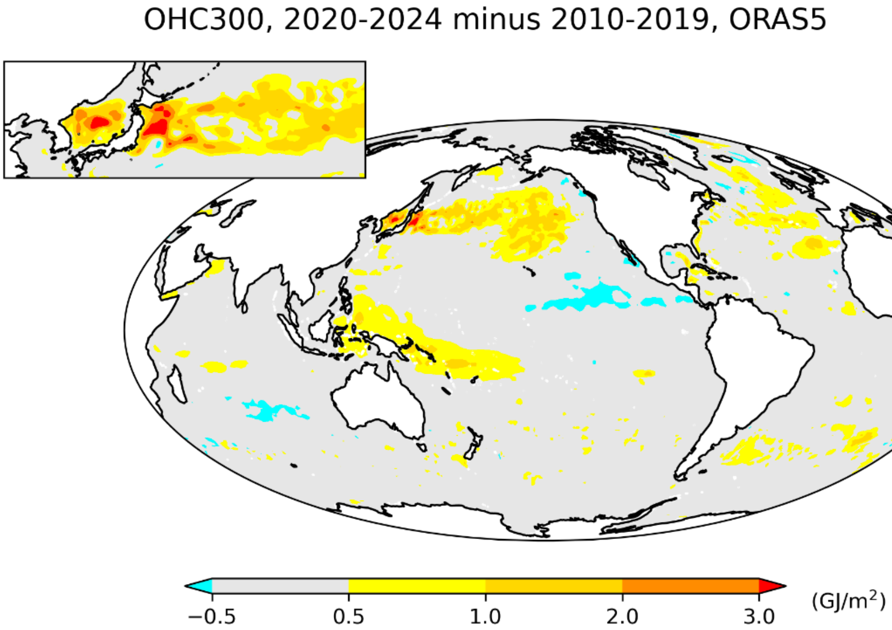

Fig. 5. Difference of 0-300 m OHC per unit area in ORAS5 between 2020-2024 and 2010-2019 periods.

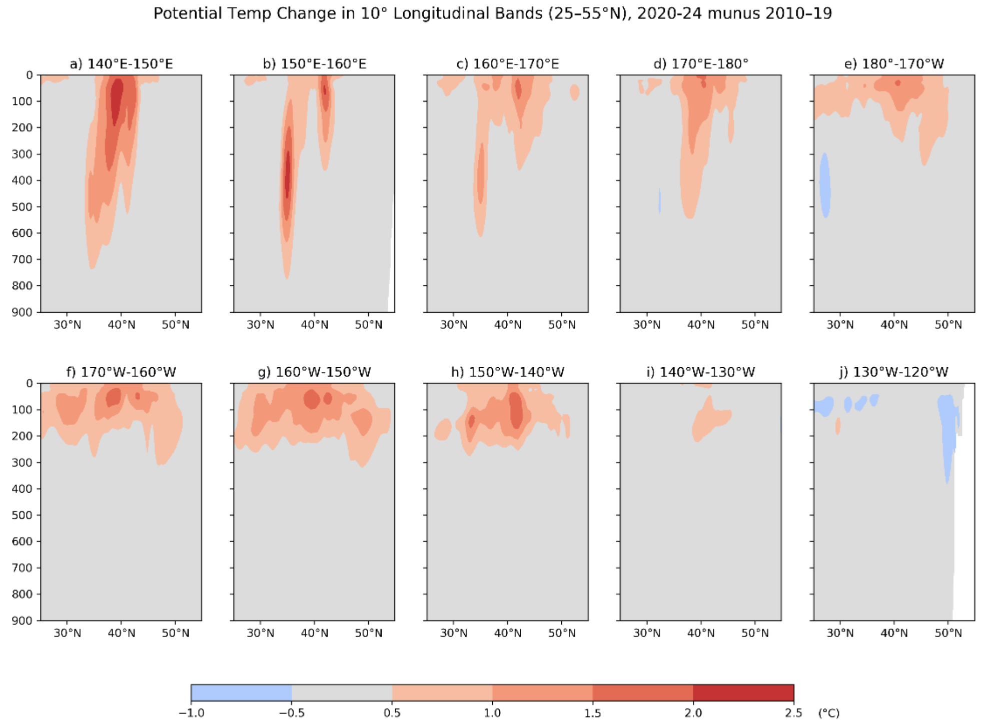

Fig. 6. Difference of potential temperature in zonal bands of 10° in longitude in ORAS5 between 2020-2024 and 2010-2019 periods.

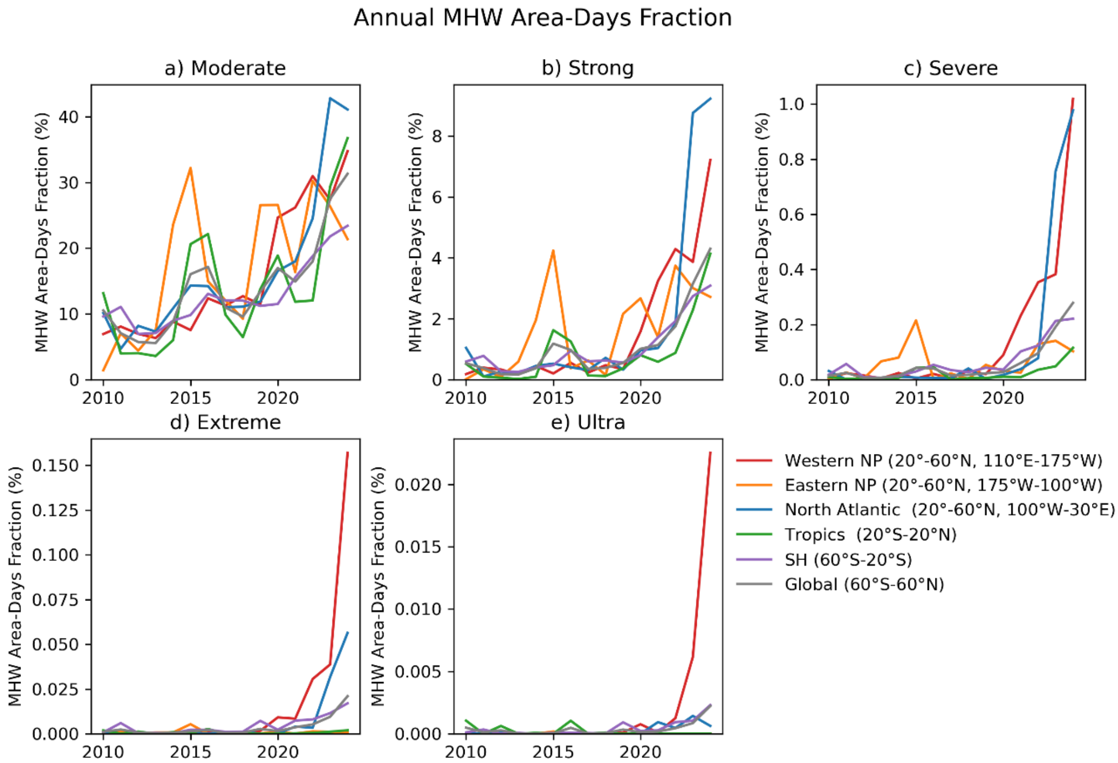

Fig. 7. Annual MHW area-days fraction for each MHW category in each basin.

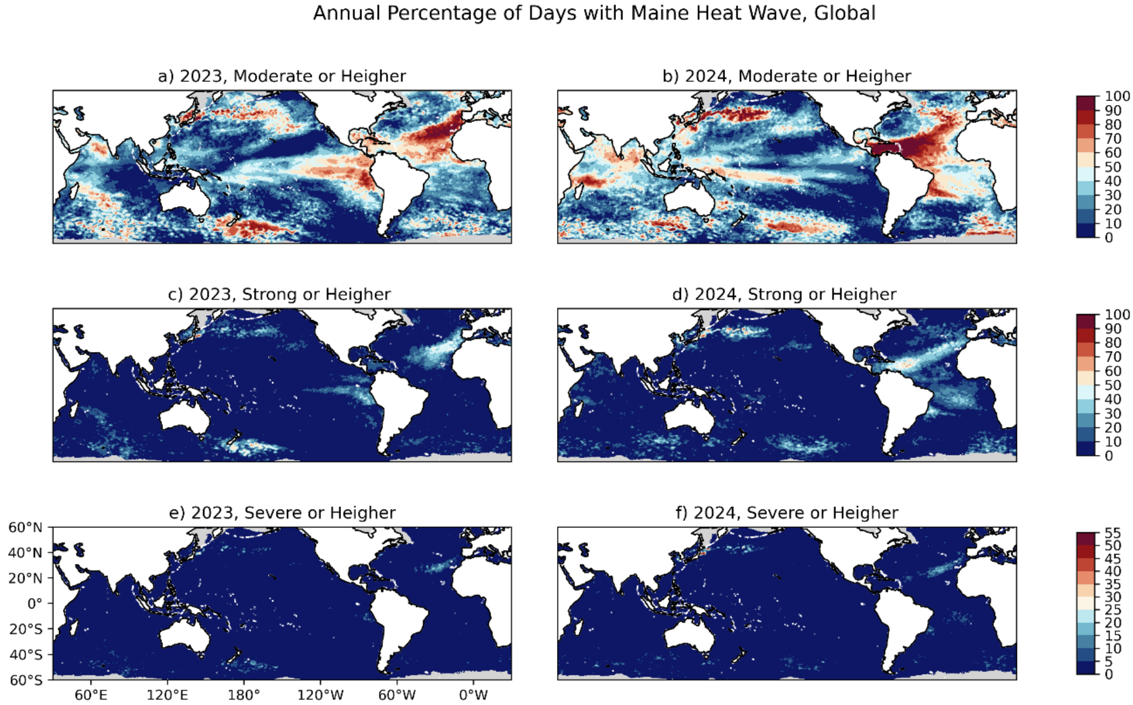

Fig. 8. Annual percentage of days with MHWs in the moderate, strong, and severe categories over the global oceans in 2023 and 2024. The percentage represents the proportion of days experiencing MHWs of the respective category or higher.

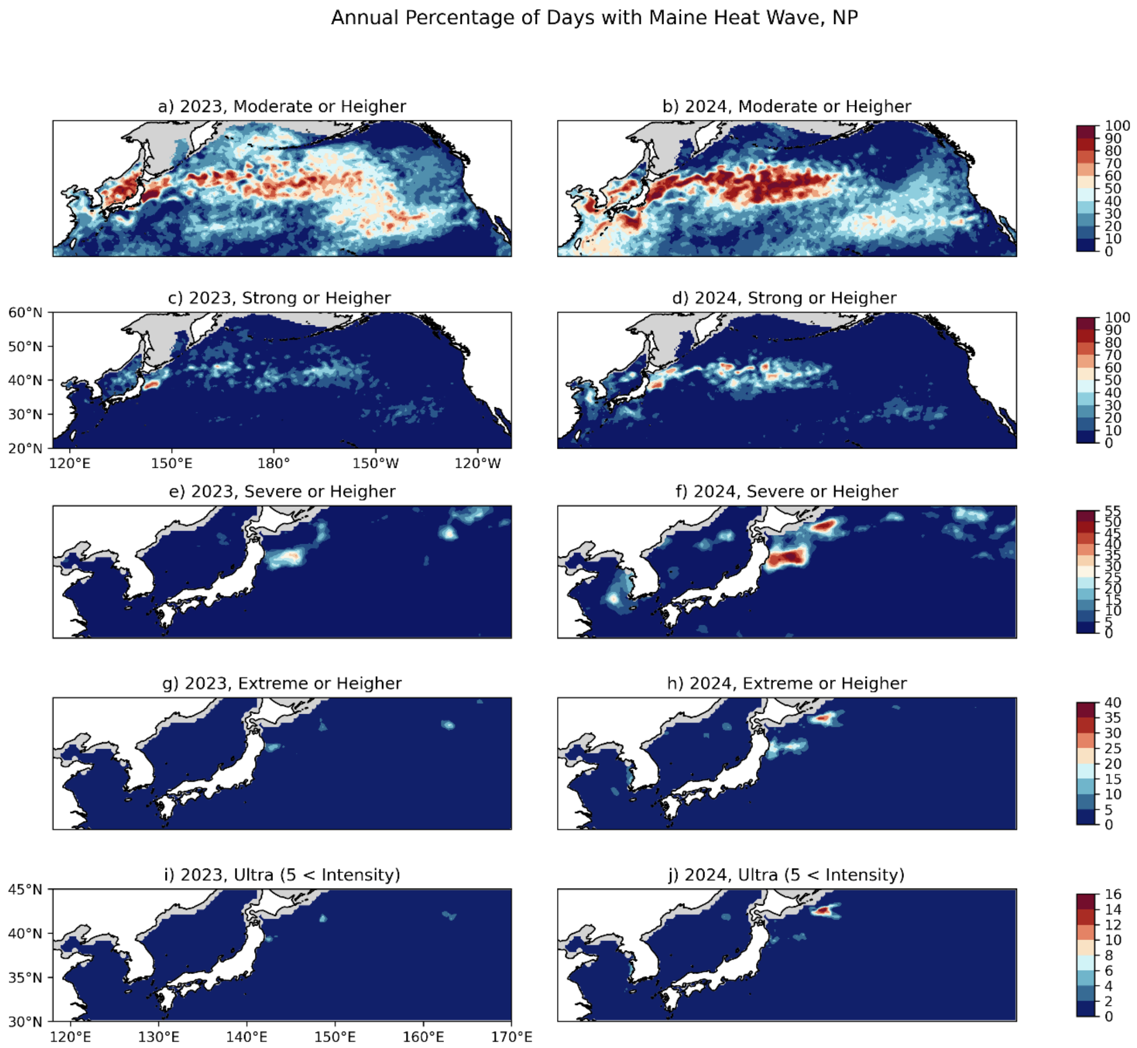

Fig. 9. Annual percentage of days with MHWs in the moderate, strong, severe, extreme, and ultra categories over the NP in 2023 and 2024. The percentage represents the proportion of days experiencing MHWs of the respective category or higher. For the bottom three panels, only a selected area of the western NP is shown, as MHWs in those categories essentially occur there.

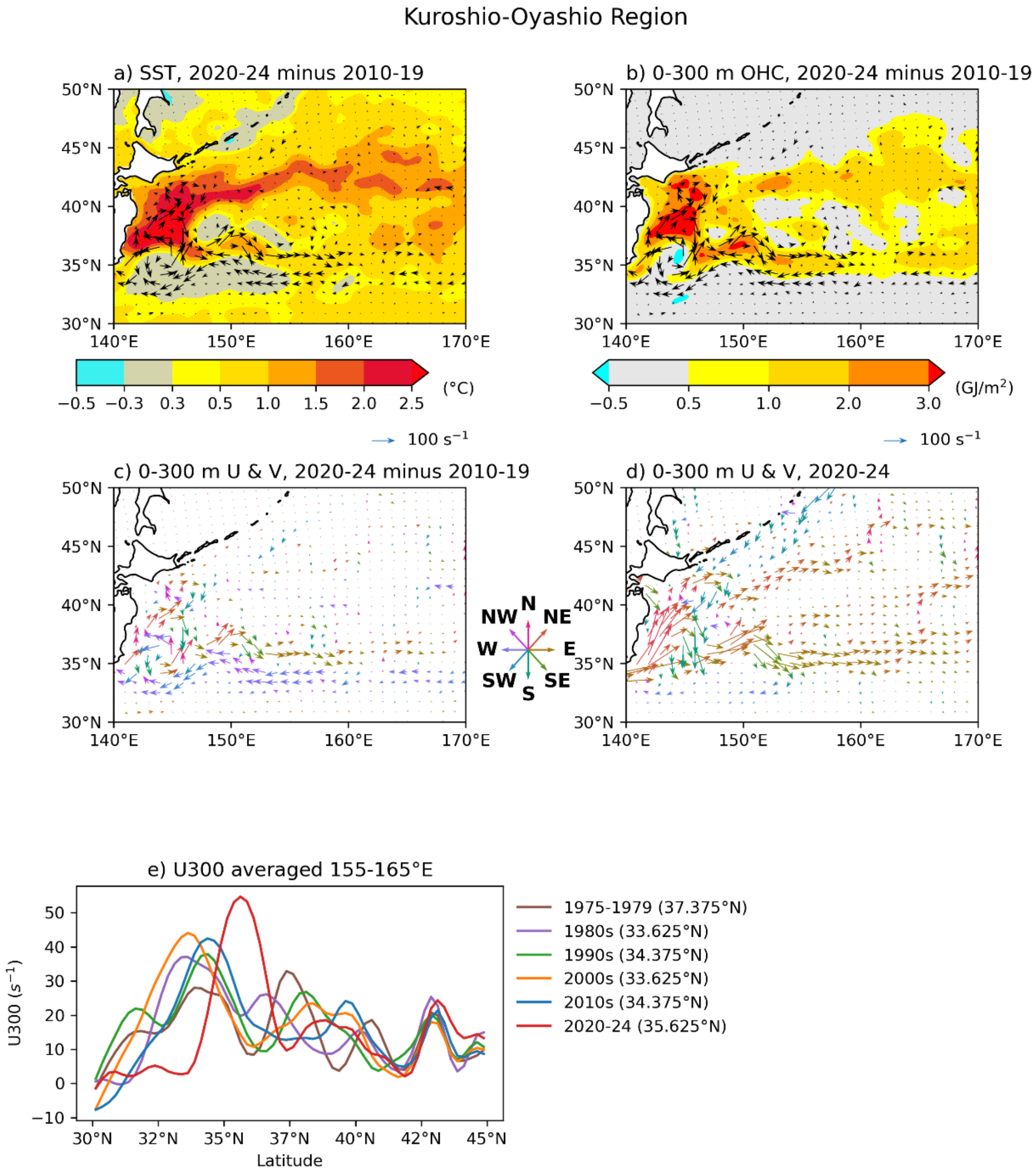

Fig. 10. Differences of (a) SST, (b) 0-300 m OHC, and (c) 0-300m ocean transport between 2020-2024 and 2010-2019 periods, (d) mean ocean transport in 2020-2024 in the Kuroshio-Oyashio region, and (e) latitudinal profiles of 0-300 m eastward transport averaged over 155-165°E in each period as shown in the legend. The vectors in panels (a) and (b) are also 0-300 m ocean transport difference shown in panel (c). Colors in panels (c) and (d) indicate the directions of the transport as shown by the reference arrows in the middle of the figure. The latitudes in parentheses in panel (e) indicate the latitude of maximum transport for each profile.

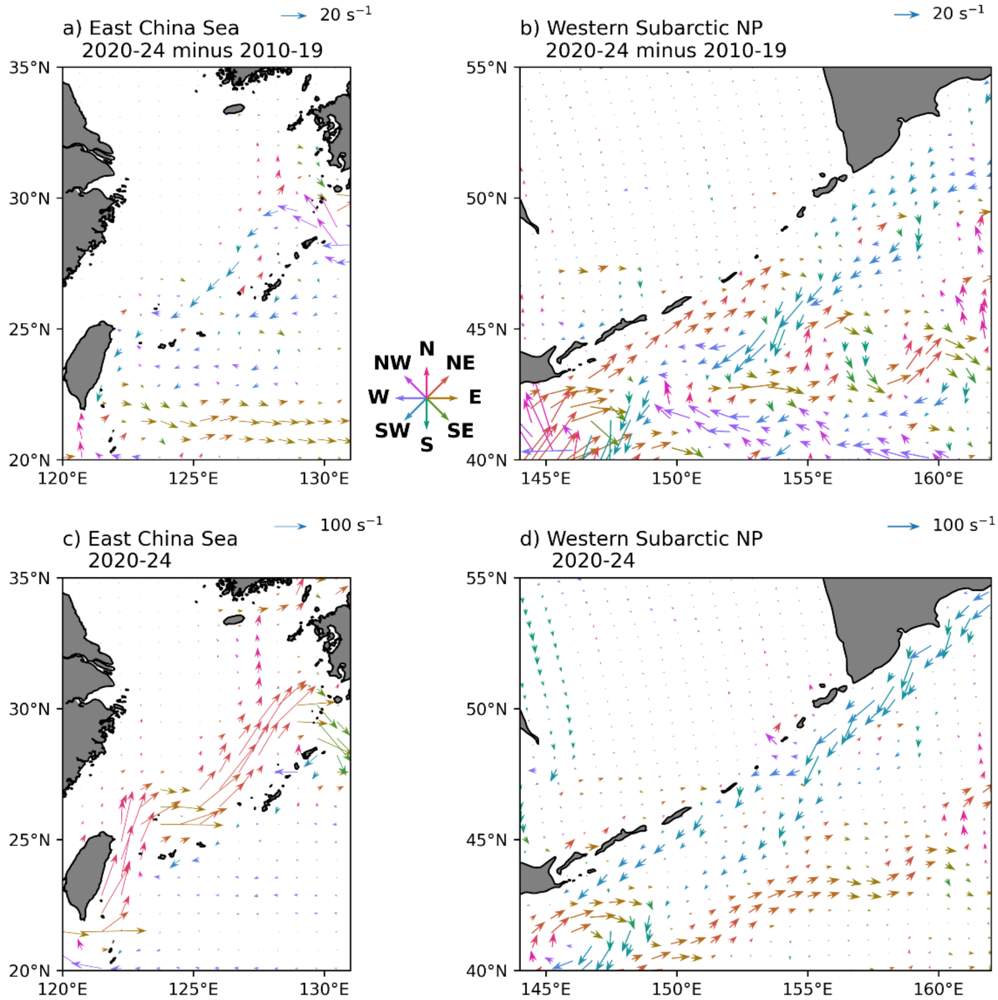

Fig. 11. (top) Difference of 0-300 m ocean transport between 2020-2024 and 2010-2019 and (bottom) the mean transport in 2020-2024 for (left) the East China Sea and (right) western subarctic NP. Colors in each panel indicate the directions of the transport as shown by the reference arrows in the middle of the figure.

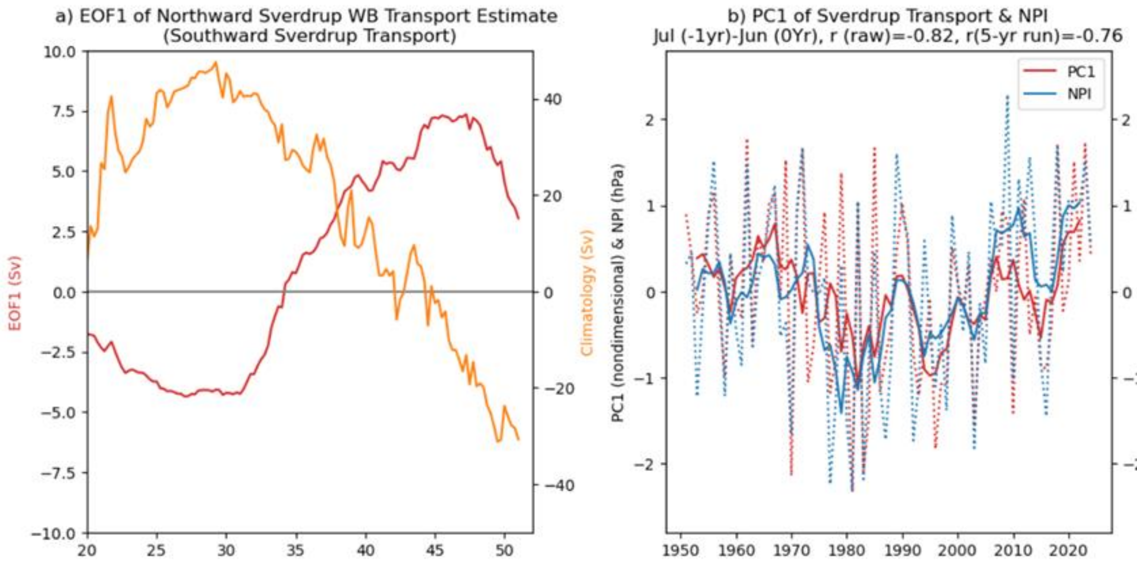

Fig. 12. Northward WB transport estimated from Sverdrup theory, showing both climatology and variability represented by the first EOF mode, which explains 42% of the variance.. (a) The climatological mean northward WB transport is shown by the yellow curve, and the spatial pattern of EOF1 for WB transport is shown by the red curve. (b) Temporal variability of the EOF1 mode (PC1) is shown by the red curve, with the NPI displayed by the blue curve. In panel (b), yearly sampled raw data (averaged from July of the previous year to June of the current year) is shown by the dashed line, while the 5-year running average is shown by the solid line. Before calculating the EOF, the transport is averaged from July of one year to June of the following year, with the year shown in the figure corresponding to the latter year.

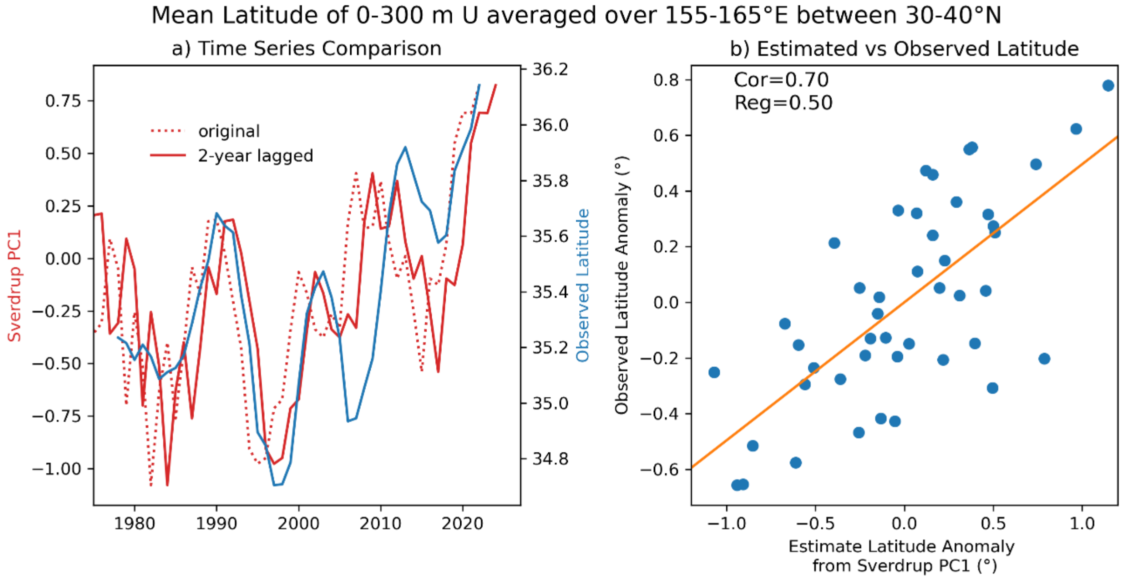

Fig. 13. (a) Time series comparison between Sverdrup PC1 (red, left-hand label) and observed transport-mean latitude of 0-300 m zonal transport averaged over 155°-165°E between 30° and 40°N (blue, right-hand label). The red dotted curve indicates the original PC1, whereas the red solid curve indicates the PC1 lagged by two years. (b) Scatter diagram between the estimated and observed latitude anomaly, corresponding to the red solid curve and blue curve in panel (a), respectively. All data smoothed by five-year running mean.

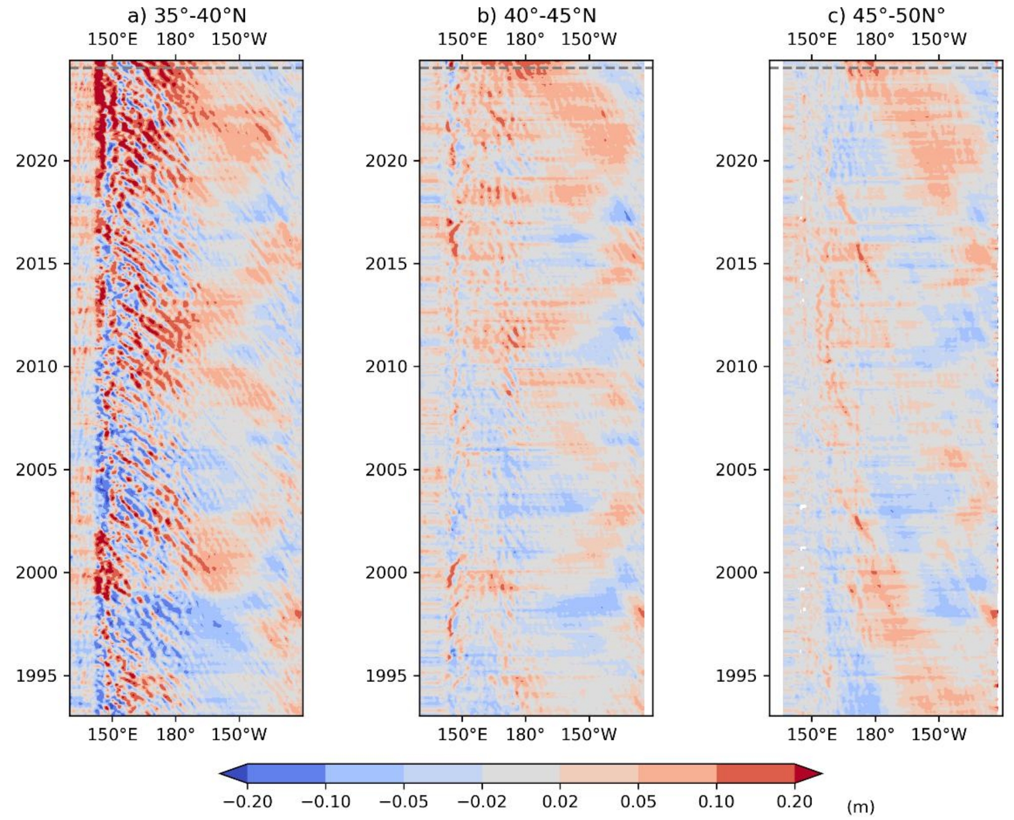

Fig. 14. **X-t diagram of satellite-derived SSH anomalies between (a) 35°-40°N, (b) 40°-45°N, and (c) 45°-50°N. Reference period is calculated from 1993 to 2019. The global mean of SSH anomalies, which exhibits an increasing trend due to global warming, is removed for each month. The horizontal dashed lines near the top of the panels indicate July 2024, the transition between delayed-time and near-real-time data.**